Spatial Instability of a Baroclinic Current with Slow Streamwise Variation

MELINDA S. PENG AND R. T. WILLIAMS

Department of Meteorology, Naval Postgraduate School, Monterey, CA 93943

(Manuscript received 27 April 1986, in final form 13 December 1986)

ABSTRACT

Spatial baroclinic instability in a mean flow with slow streamwise variation is studied with the quasi-geostrophic two-layer model. The two-scale expansion technique which was employed by Peng and Williams is used in this study. The zero-order terms give the local spatial instability solution. The next order terms determine the correction to the local solution due to the streamwise variation of the mean flow. It is found that this correction is not negligible when the β effect is large and the vertical shear is small. The results are explained with the lag effect, which was discussed by Peng and Williams. The lag effect occurs when the local solution changes its structure substantially in the streamwise direction. When the vertical shear is large or when the β effect is small, the ratio between the disturbances of the two layers is nearly uniform in the streamwise direction, even though the shear changes substantially. Thus, only a small lag effect is experienced by a disturbance as it propagates, and the streamwise effect is unimportant. The dependence of the vertical structure on the basic flow variation and other parameters is analyzed.

I. Introduction

The traditional studies of baroclinic instability in the atmosphere and in the ocean (Charney, 1947; Eady, 1949; Phillips, 1951) assume that the basic flow is uniform in the streamwise direction. Observations indicate that this is often not the case. Land–sea contrasts and topographic effects can lead to significant streamwise changes in baroclinicity. Therefore, it is important to examine the influence of streamwise variations in the basic flow on baroclinic stability theory. A basic current with streamwise variation can be obtained by adding a stationary long wave to a uniform zonal flow. Due to the mathematical nonseparability of nonparallel flow problems, either numerical integration or the multiple scale technique have been used. For example, Tupaz et al. (1978), Niehaus (1980), Frederiksen (1979), and Merkine and Balgovid (1983), have used numerical integration (including spectral space methods), and multiple scale techniques have been used by Drazin (1974), Ling and Reynolds (1973), Niehaus (1981) and Peng and Williams (1986). A review paper by Grotjahn (1984a) summarizes research on basic currents with streamwise variation. The finite amplitude behavior of disturbances, in a flow with abrupt streamwise variation from a weakly unstable region to a stable region (and vice versa) was studied by Pedlosky (1976).

Peng and Williams (1986) applied the multiple scale technique to the barotropic instability problem which had been solved numerically by Tupaz et al. (1978). Comparisons between these two results verified the accuracy of the multiple scale technique, and Peng and Williams were able to determine the influence of streamwise variation of the basic flow on growth rate, wavenumber, etc. The baroclinic instability for basic flows that change in the streamwise direction is studied here using the same technique. As in Peng and Williams, the major purpose is to obtain the difference between the local stability solution for parallel flow and the nonparallel solution.

In the analysis of parallel flows, the instability is usually examined with temporal growth for real wavenumbers so that the wave is spatially periodic and the solution is bounded in space. For nonparallel flows, it is not necessary to have spatial periodicity for boundedness. Due to advection by the basic flow and propagation of the disturbance itself, the disturbance experiences environments with different stability properties as it travels. It is appropriate in this case to consider the spatial instability. The spatial growth rate comes from the imaginary part of the wavenumber, which allows the amplitude to grow in space as the disturbance moves downstream. Physically, the temporal growth rate can be linked to the spatial growth rate by a function of the phase velocity.

The most general approach is to consider both the temporal and the spatial growth simultaneously. That is, both the wavenumber and the frequency are complex (e.g., see Merkine and Shafranek, 1980). Under some circumstances, the basic flow can support absolute instability, in which case the spatial amplification will be obscured. The concept of absolute instability was first discussed in plasma physics by Briggs (1964), and introduced to geophysical fluid dynamics by Thacker (1976) and Merkine (1977). Mathematically, the existence of absolute instability requires the van-

ishing of the complex group velocity $d\omega/dk = 0$ when the imaginary part of the frequency is positive. Physically, when the speed of the mean flow is not large relative to the shear of the flow, the envelope packet of a disturbance which is excited at some point will not be advected downstream fast enough and any point reached by the disturbance can grow exponentially in time. Therefore, for basic flows that support absolute instability, the spatially amplifying waves cannot be identified.

Thacker (1976) and Merkine (1977) obtained the criteria for absolute instability for the two-layer baroclinic model. Merkine purposed local absolute instability as a possible explanation of lee cyclogenesis, while Thacker suggested that spatial amplification of the meanders in the Gulf Stream can exist when absolute instability is not present.

Pierrehumbert (1984) used both numerical integration and an analytic approach to study a zonally varying basic flow which supports absolute instability in some region of the domain. It was found that the frequency determined by the absolute instability at the location of the maximum shear dominates the evolution of the disturbances in the domain. The growth rate determined using parallel flow theory compares favorably with those obtained from the numerical integration of the complete equations.

In the absolute instability studies mentioned above, the domains in the north–south direction were unbounded. Merkine (1977) showed that the stabilizing effect of the north–south boundaries requires a larger shear relative to the averaged mean flow to support absolute instability unless the scale of the disturbance is very large. The criteria listed as (A13) in Merkine (1977) can be obtained from the observation that for amplifying waves, the maximum spatial growth rate corresponds approximately to a frequency for which the speed of the wave is equal to the average speed of the basic flow. This criteria is verified for the parameters of this problem by direct calculation. For all the cases treated in the present paper, the basic flows do not support absolute instability. Thus, the spatial growth approach can be used effectively to study disturbances in our flow fields that contain streamwise variation. Therefore, we treat only spatial instability in the study.

This stability study uses the quasi-geostrophic two-layer baroclinic model which was originally formulated by Phillips (1951) and treated extensively by Pedlosky (1979). The two-layer model, which is very simple, has been used to capture many dynamic aspects of large-scale atmospheric flows. The model with a nonuniform basic flow is described in section 2, and the two-scale expansion procedures are given in section 3. Results for different basic flow variations are presented and discussed in section 4. In section 5, we analyze the difference in structure between the disturbances in the two layers when the vertical shear and the β parameter are changed. This analysis is used to further support the interpretation of the results in section 4. The discussion and conclusion are given in section 6.

2. The model

The two-layer quasi-geostrophic model was derived by Phillips (1951), and the notation in the present paper follows Pedlosky (1979). The model contains two immiscible, incompressible fluid layers, each with different densities ρ_1 and ρ_2, and different zonal velocities U_1 and U_2. The densities ρ_1 and ρ_2 are kept constant while the velocities U_1 and U_2 change slowly in the streamwise direction. It is observed that the characteristic length scale of the basic flow in the streamwise direction is much longer than its cross-stream characteristic length scale (an example is presented in section 4). The fluid is bounded above and below by two rigid horizontal planes. Ekman friction is incorporated into the system through vertical boundary conditions. The nondimensional potential vorticity equations are as follows:

$$\left(\frac{\partial}{\partial t}+\frac{\partial\psi_n}{\partial x}\frac{\partial}{\partial y}-\frac{\partial\psi_n}{\partial y}\frac{\partial}{\partial x}\right)(\nabla^2\psi_n \pm F(\psi_2-\psi_1)+\beta y) = -r\nabla^2\psi_n, \quad (2.1)$$

where $n = 1$ and 2 denote the upper and lower layers, respectively. When there are two signs appearing before a term, as in (2.1), the upper sign belongs to the equation for $n = 1$ and the lower sign belongs to the equation for $n = 2$. The Froude number F is the same for both layers since the two layers considered here are of equal ambient depth. The nondimensional parameters are defined as follows:

$$F=\frac{f_0^2L^2}{g[(\rho_2-\rho_1)/\rho_0]D} \quad (2.2)$$

$$\beta=\frac{\beta_0L^2}{U} \quad (2.3)$$

$$r=\frac{E_v^{1/2}}{R_0}, \quad (2.4)$$

where β_0 is the dimensional beta, E_v is the Ekman number, Ro is the Rossby number and D is the layer depth.

For channel geometry, the kinematic boundary conditions at the walls give

$$\frac{\partial\psi_n}{\partial x}=0 \quad \text{at} \quad y=0,1. \quad (2.5)$$

The total streamfunction ψ_n is

$$\psi_n=\bar{\psi}_n+\psi'_n, \quad (2.6)$$

where $\bar{\psi}_n$ is the basic state streamfunction and ψ'_n represents the streamfunction for the disturbance field.

3. Mathematical formulation

The basic state is a nondivergent flow which varies "slowly" with x. A long spatial scale coordinate X is defined by introducing a small parameter ϵ, so that

$$X = \epsilon x, \tag{3.1}$$

which measures the streamwise variation of the basic flow. The basic flows U_1 and U_2 are constants with respect to the y coordinate, and they vary with the long space scale X. For nondivergent basic flow,

$$U_n(X) = -\frac{\partial \bar{\psi}_n}{\partial y}, \tag{3.2}$$

it follows that

$$\bar{\psi}_n = -U_n(X)y, \tag{3.3}$$

$$\frac{\partial \bar{\psi}_n}{\partial x} = \epsilon \frac{\partial \bar{\psi}_n}{\partial X} = \epsilon V_n = -\epsilon \frac{\partial U_n}{\partial X} y. \tag{3.4}$$

Now we linearize (2.1) with respect to $\bar{\psi}_n$ and then use the relations above to obtain

$$\left(\frac{\partial}{\partial t} + \epsilon V_n \frac{\partial}{\partial y} + U_n \frac{\partial}{\partial x}\right)(\nabla^2 \psi'_n \pm F(\psi'_2 - \psi'_1) + \beta y) + \frac{\partial \psi'_n}{\partial x}\beta$$
$$- \epsilon^2 \frac{\partial \psi'_n}{\partial x}\frac{\partial^2 U_n}{\partial Z^2} - \frac{\partial \psi'_n}{\partial y}\epsilon^3 \frac{\partial^2 V_1}{\partial X} \pm \frac{\partial \psi'_n}{\partial x} F(U_1 - U_2)$$
$$\mp \frac{\partial \psi'_n}{\partial y}\epsilon(V_2 - V_1)F = -r\nabla^2 \psi'_n. \tag{3.5}$$

The normal mode solution for the disturbance ψ'_n in Eq. (3.5) is

$$\psi'_n = \phi_n(X, y)e^{i\theta} \tag{3.6}$$

where θ is the phase angle, which is treated as an independent variable (Nayfeh et al., 1974). The wavenumber k and frequency ω are obtained from the relations

$$\frac{\partial \theta}{\partial X} = \frac{1}{\epsilon} k(X), \tag{3.7}$$

$$\frac{\partial \theta}{\partial t} = -\omega. \tag{3.8}$$

The asymptotic expansions of k and ϕ in terms of ϵ (Benney and Rosenblat, 1964) are as follows:

$$k = k_0(X) + \epsilon k_1(X) + \epsilon^2 k_2(X) + \cdots \tag{3.9}$$

$$\phi_n = \phi_n^{(0)}(X, y) + \epsilon \phi_n^{(1)}(X, y) + \epsilon^2 \phi_n^{(2)}(X, y) + \cdots. \tag{3.10}$$

If we substitute the relations (3.6)–(3.10) into (3.5) and (2.5), we obtain a sequence of equations for different orders of ϵ.

O(1) problem

$$-(U_n k_0 - \omega)\left(\frac{\partial^2 \phi_n^{(0)}}{\partial y^2} - k_0^2 \phi_n^{(0)} \pm F(\phi_2^{(0)} - \phi_1^{(0)})\right)$$
$$+ k_0 \phi_n^{(0)}\beta \pm k_0 \phi_n^{(0)} F(U_1 - U_2)$$
$$- ir\left(\frac{\partial^2 \phi_n^{(0)}}{\partial y^2} - k_0^2 \phi_n^{(0)}\right) = 0 \tag{3.11}$$

$$\phi_n^{(0)} = 0 \quad \text{at} \quad y = 0, 1. \tag{3.12}$$

Since the coefficients in Eq. (3.11) are not functions of y, $\phi_n^{(0)}$ can be sought in the form

$$\phi_n^{(0)} = \Phi_n^{(0)}(X) \sin m\pi y \tag{3.13}$$

which satisfies the boundary condition (3.12) automatically. When (3.13) is substituted into Eq. (3.11), two algebraic equations for unknowns $\Phi_1^{(0)}$ and $\Phi_2^{(0)}$ are obtained:

$$i(-\omega + U_n k_0)[-(k_0^2 + m^2\pi^2)\Phi_n^{(0)} \pm F(\Phi_2^{(0)} - \Phi_1^{(0)})]$$
$$+ ik_0 \Phi_n^{(0)} \pm ik_0 \Phi_n^{(0)} F(U_1 - U_2) - r(k_0^2 + m^2\pi^2)\Phi_n^{(0)} = 0. \tag{3.14}$$

The determinant of the coefficients of $\Phi_1^{(0)}$ and $\Phi_2^{(0)}$ in (3.14) must vanish in order for $\Phi_1^{(0)}$ and $\Phi_2^{(0)}$ to have nontrivial solutions. That is,

$$-(U_1 k_0 - \omega)(U_2 k_0 - \omega)(2FK^2 + K^4)$$
$$+ k_0(F + K^2)[\beta k_0(U_2 + U_1) - Fk_0(U_1 - U_2)^2 - 2\omega\beta]$$
$$+ irK^2(F + K^2)[k_0(U_2 + U_1) - 2\omega]$$
$$- k_0^2[\beta^2 - F^2(U_1 - U_2)^2] - 2irk_0 K^2 \beta + r^2 K^4 = 0 \tag{3.15}$$

where

$$K^2 = k_0^2 + m^2\pi^2. \tag{3.16}$$

Equation (3.15) is the stability equation for parallel baroclinic flow in the two-layer model.

The vertical structure of the disturbance solution at this order is determined by the ratio between $\Phi_1^{(0)}$ and $\Phi_2^{(0)}$, defined as R which is obtained from (3.14).

$$R = \frac{\Phi_2^{(0)}}{\Phi_1^{(0)}}$$
$$= \frac{(U_1 k_0 - \omega)(F + K^2) - k_0[\beta + F(U_1 - U_2)] - irK^2}{(U_1 k_0 - \omega)F}$$
$$= Ae^{i\theta_p} \tag{3.17}$$

where A is the amplitude ratio and θ_p gives the phase angle difference between the two layers.

For conventional temporal instability, the wavenumber k is a real constant in (3.15), and we seek a complex frequency ω. For spatial instability, the frequency ω is a real constant and a complex wavenumber k is sought where the imaginary part of k will be the spatial growth rate. Here, (3.15) will be solved for com-

plex k as a function of X. This gives the local solution for each X.

Without loss of generality, $\Phi_1^{(0)}$ is chosen as a constant for all X. Therefore,

$$\frac{\partial \phi_1^{(0)}(X,y)}{\partial X} = \frac{\partial \Phi_1^{(0)}}{\partial X} \sin m\pi y = 0 \tag{3.18}$$

$$\frac{\partial \phi_2^{(0)}(X,y)}{\partial X} = \Phi_1^{(0)} \frac{\partial R}{\partial X} \sin m\pi y. \tag{3.19}$$

O(ϵ) problem

$$\begin{aligned} & i(-\omega + U_n k_0)\left[-k_0^2 \phi_n^{(1)} + \frac{\partial^2 \phi_n^{(1)}}{\partial y^2} \pm F(\phi_2^{(1)} - \phi_1^{(1)})\right] \\ & + ik_0 \phi_n^{(1)} \beta \pm ik_0 \phi_n^{(1)} F(U_1 - U_2) \\ & + r\left(-k_0^2 + \phi_n^{(1)} + \frac{\partial^2 \phi_n^{(1)}}{\partial y^2}\right) \\ & = -i(U_n k_0 - \omega)\left[-2k_0 k_1 \phi_n^{(0)} + 2k_0 i \frac{\partial \phi_n^{(0)}}{\partial X} + \frac{\partial k_0}{\partial X} i \phi_n^{(0)}\right] \\ & - \left(V_n \frac{\partial}{\partial y} + iU_n k_1 + U_n \frac{\partial}{\partial X}\right)\left[-k_0^2 \phi_n^{(0)} + \frac{\partial^2 \phi_n^{(0)}}{\partial y^2}\right. \\ & \left. \pm F(\phi_2^{(0)} - \phi_1^{(0)})\right] - ik_1 \phi_n^{(0)} \beta + \frac{\partial \phi_n^{(0)}}{\partial X} \beta \\ & \mp F(U_2 - U_1)\left(ik_1 \phi_n^{(0)} + \frac{\partial \phi_n^{(0)}}{\partial X}\right) \pm F(V_2 - V_1) \frac{\partial \phi_n^{(0)}}{\partial y} \\ & + r\left(2k_0 k_1 \phi_n^{(0)} + 2ik_0 \frac{\partial \phi_n^{(0)}}{\partial X} + i\phi_n^{(0)} \frac{\partial k_0}{\partial X}\right) \end{aligned} \tag{3.20}$$

$$\phi_n^{(1)} = 0 \quad \text{at} \quad y = \pm 1. \tag{3.21}$$

The left-hand sides of (3.20) have the same structure as in the O(1) problem, (3.11). Therefore, Φ_n^1 has a homogeneous solution with the same structure as $\Phi_n^{(0)}$, since the boundary conditions are the same. Let

$$\phi_n^{(1)} = \Phi_n^{(1)}(X) \sin m\pi y. \tag{3.22}$$

After we substitute (3.22) and (3.13) into (3.20), we require that the terms on the right-hand side that are proportional to $\sin m\pi y$ (i.e., the homogeneous solution) vanish in order to satisfy the solvability condition (Nayfeh, 1979). In abbreviated form, they can be written as

$$\begin{aligned} -R\Phi_1^{(1)} + \Phi_2^{(1)} &= H_1 \\ \Phi_1^{(1)} - \frac{1}{R}\Phi_2^{(1)} &= H_2 \end{aligned} \tag{3.23}$$

where H_1 and H_2 are given in the Appendix and R is defined in (3.17). The solvability condition is

$$\begin{vmatrix} -R & H_1 \\ 1 & H_2 \end{vmatrix} = 0. \tag{3.24}$$

Since k_1 is the only unknown in (3.24), it can be solved as

$$k_1 = \frac{S_1}{S_2}, \tag{3.25}$$

where S_1 and S_2 are the expressions containing properties of the O(1) problem. These are also given in the Appendix.

To O(ϵ) accuracy, the spatial growth rate of the streamwise solution is

$$\mathrm{Im}k = \mathrm{Im}(k_0 + \epsilon k_1), \tag{3.26}$$

and the local wavenumber is

$$\mathrm{Re}k = \mathrm{Re}(k_0 + \epsilon k_1). \tag{3.27}$$

4. Experiments and results

Although the streamwise variation of the basic flow is small in comparison with the cross-channel variation, the total downstream variation can be large enough to be comparable to the observed variations. As an illustration, the climatological zonal mean winds at levels 200 and 700 mb of the Northern Hemisphere for the months of December, January and February, which were analyzed by Oort (1983), are presented in Fig. 1. Although the climatological mean does not represent the true basic state, this diagram does illustrate the general profile for streamwise variation. We focus our attention on the jet centered over eastern Asia; the variation of the jet in the north–south direction is not included. The appropriate scales and the resulting nondimensional parameters are as follows:

$$\begin{aligned} L &\quad 1500\,\mathrm{km}, \\ D &\quad 5\,\mathrm{km}, \\ U &\quad 30\,\mathrm{m\,s^{-1}}, \\ \epsilon &\quad 0.2, \\ \beta &\quad 1.5, \\ F &\quad 10.0, \\ r &\quad 0.0. \end{aligned} \tag{4.1}$$

The parameters β and r are varied in later cases.

The nondimensional basic flows U_1 and U_2 in streamwise direction are prescribed in general as

$$U_1 = a + b\,\mathrm{sech}(X + h_1) \tag{4.2}$$

$$U_2 = c + d\,\mathrm{sech}(X), \tag{4.3}$$

where X is the long spatial coordinate which is defined in (3.1). The constants a, b, c and d determine the magnitudes of the basic flows and the relative shear between the two layers (U_1–U_2). Variations of these constants allow different profiles of the streamwise variation for the jet. The location of the maximum wind region in one layer can be shifted relative to the

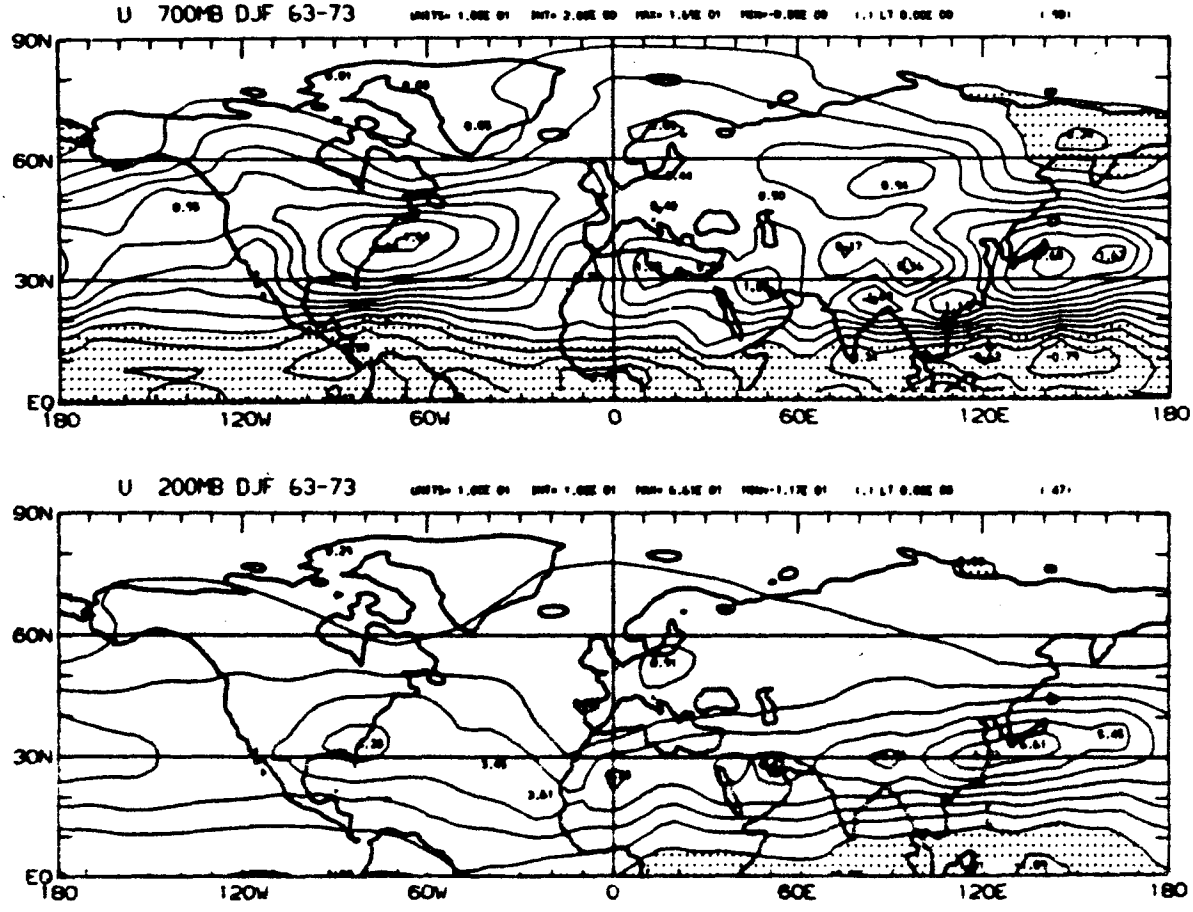

FIG. 1. Mean wintertime zonal wind speed U at (a) 700 mb; (b) 200 mb: contour interval 5 m sec^{-1} adopted from Oort (1983).

maximum in the other layer. Usually, the upper-layer structure lags the structure of the lower layer. Examination of Fig. 1 indicates that the jet maximum at the 200-mb level is located along 125°E, while the jet maximum at 700 mb is located along 150°E. In expression (4.2), constant h_1 determines the longitudinal shift of the streamwise variation of the basic flows between the two layers. To understand the problem in a systematic way, some of the constants in (4.2) and (4.3) are set to zero first so that simple cases can be isolated. In the diagrams where the mean flows are plotted as functions of X, the solid line is the upper-layer mean flow and the dashed line is the lower-layer mean flow. In diagrams where the streamwise and local solutions are presented, the solid line refers to the local parallel flow solution obtained from the O(1) problem and the dashed line refers to the streamwise (nonparallel) solution. The streamwise solution is the sum of the local solution and the O(ϵ) correction, i.e., Eqs. (3.26) and (3.27).

It is informative to review the previous study by Peng and Williams (1986) which examined the mechanism of barotropic instability in a jet with streamwise variation. In their discussion, the difference between the spatial growth rate with streamwise variation and the local spatial growth rate is related to two effects. First, a lag effect occurs when the structure of the disturbance calculated by local parallel flow theory varies downstream due to the variation in the basic flow. As the disturbance propagates through regions of different basic flow, there is a lag in the adjustment of the disturbance structure to the local structure obtained from parallel flow theory. In regions where the parallel flow growth rate increases downstream, the nonparallel growth rate will be smaller than the local parallel growth rate and vice versa. The second effect depends on the relative phase speed between the streamwise solution and the local solution. If the phase speed for the streamwise solution is larger (smaller) than the phase speed for the local solution, the disturbance will have less (more) time to grow in space and the streamwise growth rate will be smaller (larger) than the local growth rate.

a. Case 1

In this case, h_1 is set to zero so that there is no longitudinal shift of the basic flow structure between the

layers. We further keep the upper-layer flow constant and only allow the basic flow in the lower layer to vary downstream, i.e.,

$$U_1 = 2.0,$$

$$U_2 = 1.1 - \text{sech}(X),$$

$$U_1 - U_2 = 0.9 + \text{sech}(X). \qquad (4.4)$$

The speeds U_1 and U_2 are plotted as functions of X in Fig. 2, where X is between -3.0 and 3.0. The vertical shear, (U_1-U_2), reaches a maximum at $X = 0$. The streamwise and local spatial growth rates for these basic flows are presented in Fig. 3. The solid line for the parallel flow solution and the dashed line which is the streamwise solution are almost identical in this case. Thus, the streamwise variation of the basic flow causes only a very small correction to the local growth rate.

Let us examine the two effects discussed in Peng and Williams (1986) to explain the present results. The streamwise and local phase speeds are plotted in Fig. 4. These two quantities are also indistinguishable, indicating that the effect due to different phase speeds (the second effect in Peng and Williams, 1986) is unimportant. The local vertical structure of the disturbance, determined by the ratio between solutions for the upper and the lower layers, is expressed as R in (3.17). This ratio, determined locally at each point as function of X, is a complex variable and can be represented by its amplitude A and phase angle θ_p. The two quantities for this case are given in Fig. 5a and 5b respectively. Although the vertical shear varies in the downstream direction (Fig. 2), it is interesting to note that the phase angle is almost the same everywhere and the amplitude changes only slightly. Due to this very small variation in the vertical structure, the disturbance does not need time (or space) to adjust itself to the local structure and no lag effect is experienced. This explains why the growth rates for the streamwise and local solutions are almost identical.

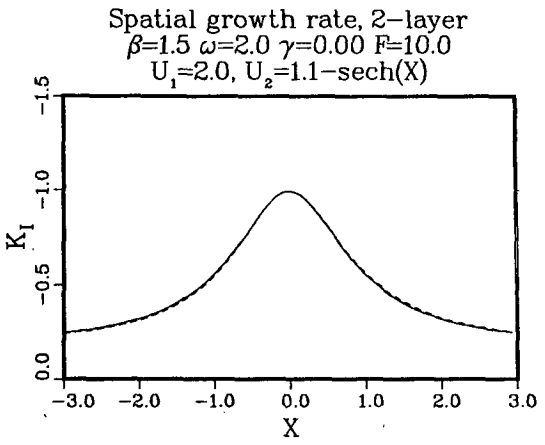

FIG. 3. Local (solid line) and streamwise (dashed line) spatial growth rates for the basic flows shown in Fig. 2 in case 1.

b. Case 2

In the second case, the basic flow for the upper layer varies while that for the lower layer remains constant. The profiles (Fig. 6) are given by

$$U_1 = 1 + \text{sech}(X),$$

$$U_2 = 0.9,$$

$$U_1 - U_2 = 0.1 + \text{sech}(X). \qquad (4.5)$$

The streamwise variation of the vertical shear in this case is the same as in case 1, but the magnitude of the shear is smaller everywhere. The phase speeds for the streamwise and local solutions are essentially the same as those in case 1 (not shown), so that the streamwise effect due to different phase speeds mentioned above contributes little to the total solution. The local structures of the disturbances are given in Fig. 7 as a function of X. Both the phase angle (7a) and the amplitude (7b)

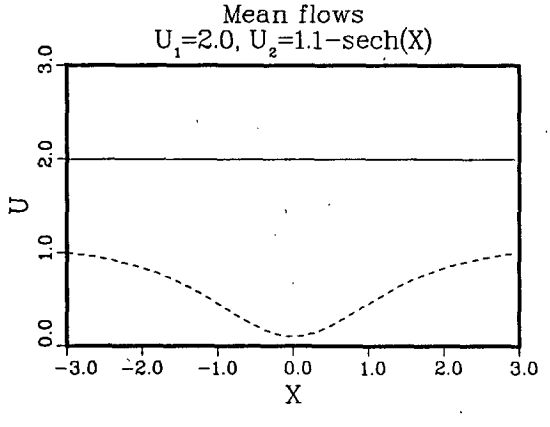

FIG. 2. Variations of the upper and lower layer mean flow U_1 (solid line) and U_2 (dashed line) as functions of X for case 1.

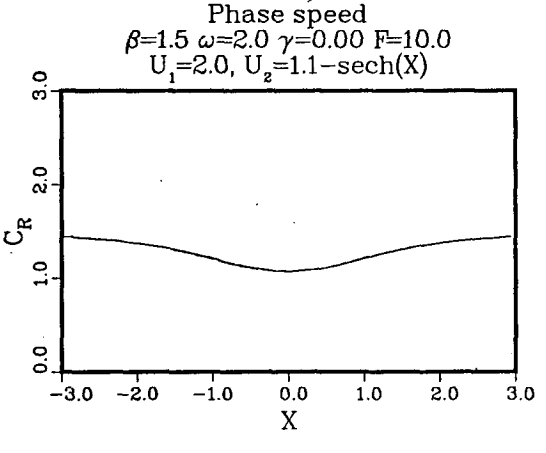

FIG. 4. Local (solid line) and streamwise (dashed line) phase speeds for case 1 as in Fig. 2.

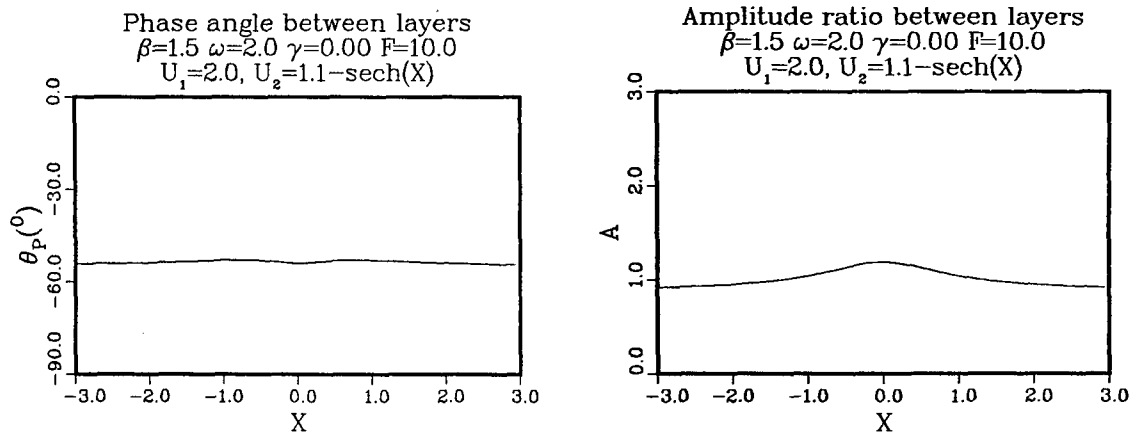

FIG. 5. Local vertical structure of the disturbance as function of X. (a) Phase angle between the upper and lower layers; (b) amplitude ratio for case 1.

show streamwise variation, especially in the entrance and outflow regions. This indicates that a lag effect is expected. The spatial growth rates in Fig. 8 clearly show the difference between the nonparallel and local solutions which is caused by the lag effect. The downstream effect, from the O(ϵ) correction, is proportional to the first derivative of the O(1) properties with respect to X, as was discussed in Peng and Williams (1986a). With the symmetric properties of the O(1) solution, the O(ϵ) correction is antisymmetric as observed.

c. Case 3

In this case, the flows in the upper and the lower layer change simultaneously in the streamwise direction. The profiles, displayed in Fig. 9, are:

$$U_1 = 1 + \text{sech}(X),$$

$$U_2 = 0.6 + 0.4\ \text{sech}(X),$$

$$U_1 - U_2 = 0.4 + 0.6\ \text{sech}(X). \tag{4.6}$$

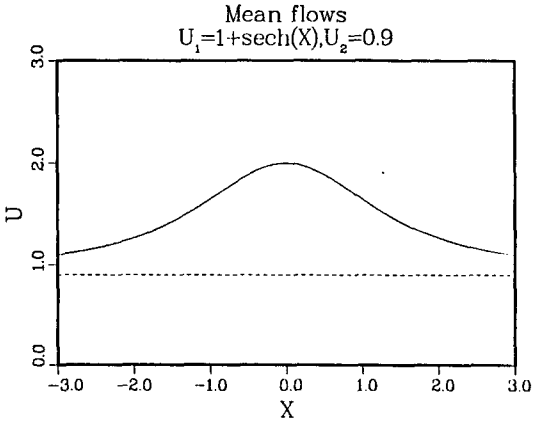

FIG. 6. U_1 and U_2 variations for case 2.

If temporal growth were sought, the maximum growth rate region would be located at the place where the vertical shear is maximum, i.e., $X = 0$ in this case. This is not always true for the spatial growth rate. Physically, the temporal growth can be linked to the spatial growth by

$$k_I = -\frac{\omega_I}{C_R}, \tag{4.7}$$

where C_R is the phase speed, ω_I the temporal growth rate and k_I is the spatial growth rate.

In general, as discussed in Peng and Williams (1987), this equation can be treated only as a link between these two types of instability and precise values of one growth rate cannot be obtained from the other using this equation. However, for the present model, Eq. (4.7) does provide very accurate results. In this case, the dispersion relation for these two types of instability is identical with the relation $\omega = k \cdot C$.

Since the phase velocity C_R is proportional to the averaged flow speed, from (4.7), the spatial growth rate will be smaller for the same shear when the averaged mean flow is larger. In this case, the parallel growth rate which is the solid line in Fig. 10 has a local minimum at the center point where the shear is a maximum. The streamwise solution represented by the dashed line in Fig. 10 is very close to the parallel solution. The difference between the parallel and nonparallel phase speeds are small (not shown), with the nonparallel phase speed slightly slower than the parallel phase speed upstream of $X = 0$ and slightly faster downstream. The amplitude of the vertical difference is almost uniform as in Fig. 11b, but the phase difference changes substantially (Fig. 11a). In order to have a significant lag effect, both the amplitude and the phase of the vertical difference have to vary substantially in the streamwise direction. Therefore, in this case, the vertical disturbance structure leads to a small lag effect (Fig. 10).

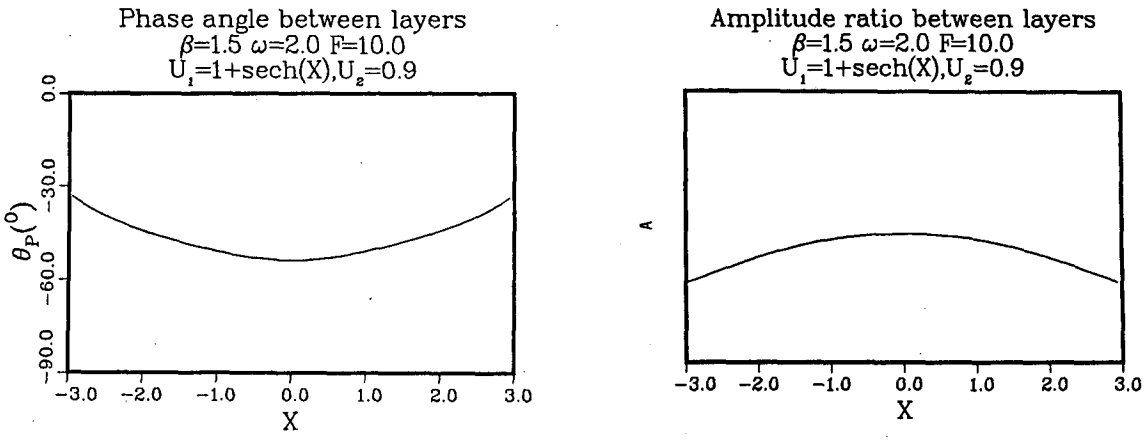

FIG. 7. (a) Phase angle between the upper and lower layer; (b) amplitude ratio for case 2.

d. Case 4

The variation of the mean flow in this case is similar to case 3, but the maximum speed region is shifted for different layers. Referring to Fig. 1, the upper flow lags the lower layer by approximately $\frac{1}{6}$ of the length of the domain considered. The profiles, which are plotted in Fig. 12, are

$$U_1 = 1 + \text{sech}(X+1),$$

$$U_2 = 0.3 + 0.4\ \text{sech}(X),$$

$$U_1 - U_2 = 0.7 + \text{sech}(X+1) - 0.4\ \text{sech}(X). \quad (4.8)$$

In Fig. 13, the spatial growth rate has a minimum near $X = 0.3$ and the nonparallel effect shows the result expected by examining the structure variation in Fig. 14.

e. Case 5

In this case, the upper flow has the same value as in case 4, but the speed of the lower layer is increased so that the magnitude of the vertical shear is decreased (Fig. 15), i.e.,

$$U_1 = 1 + \text{sech}(X+1),$$

$$U_2 = 0.6 + 0.7\ \text{sech}(X),$$

$$U_1 - U_2 = 0.4 + \text{sech}(X+1) - 0.7\ \text{sech}(X). \quad (4.9)$$

In Fig. 16, the parallel growth rate (solid line) is similar to that of case 4, yet, very significant nonparallel effects (dashed line) are observed near the minimum growth rate region, i.e., $X = 0.5$. The phase speed in Fig. 17 indicates a slightly slower phase speed for the nonparallel flow upstream from $X = 0.5$ and slightly faster phase speed downstream. From the second effect

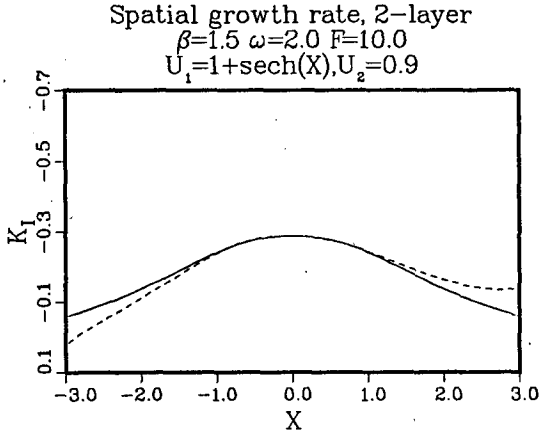

FIG. 8. Spatial growth rate for local (solid line) and streamwise (dashed line) solutions for case 2 as in Fig. 6.

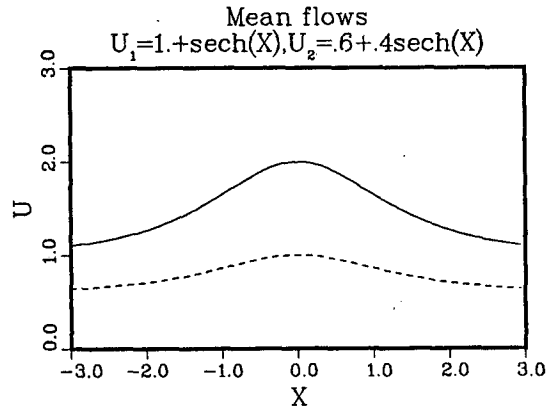

FIG. 9. U_1 and U_2 profiles for case 3.

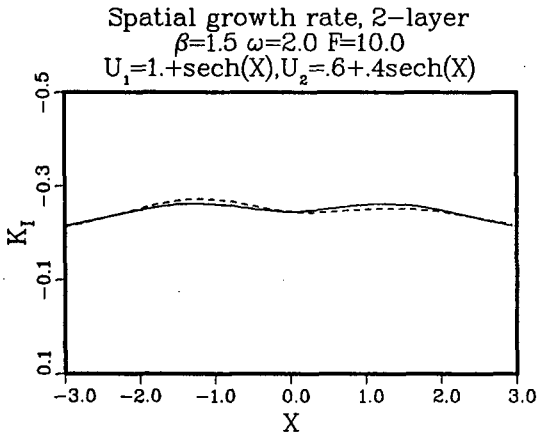

FIG. 10. Local (solid line) and streamwise (dashed line) spatial growth rate for case 3 as in Fig. 9.

proposed by Peng and Williams (1986), the nonparallel growth rate would be slightly larger than the parallel growth rate upstream of $X = 0.5$ and vice versa downstream. Furthermore, in Fig. 18, both the phase angle and the amplitude of the vertical difference in disturbance structure show substantial variation near the minimum shear region at $X = 0.5$. Thus, lag effect makes the dominant contribution to the nonparallel effect in this region.

When the frictional coefficient r increases from 0.0 to 0.1, the overall growth rate decreases and the lag effect also decreases.

The five cases presented above indicate that the two effects discussed in Peng and Williams (1986) can successfully explain the streamwise effects obtained in the present study. A major result is that, although the streamwise variation of the basic flow considered here is twice the variation in previous barotropic study (i.e., $\epsilon = 0.2$ vs $\epsilon = 0.1$), the nonparallel solutions are very close to the local parallel solutions for most of the cases considered. The smallness of downstream effects comes from the fact that the vertical structure of the disturbances is essentially insensitive to variations in the vertical shear. In the next section, we will analyze the dependency of the vertical structure on the shear and other parameters.

5. Dependency of the vertical structure of the disturbance on the shear

Equation (3.14) contains two separate equations for the disturbances of the upper ($n = 1$) and lower ($n = 2$) layers. The ratio R between the disturbances in the upper and lower layers, which is given by (3.17), can be obtained by setting either $n = 1$ or $n = 2$ in (3.14). An alternative is to add the $n = 1$ and $n = 2$ equations from (3.14), which gives

$$\frac{\Phi_1^{(0)}}{\Phi_2^{(0)}} = -\frac{-K^2(U_2k_0-\omega)+k_0\beta+irK^2}{-K^2(U_1k_0-\omega)+k_0\beta+irK^2}. \tag{5.1}$$

For simplification, the frictional coefficient r is set equal to zero in (5.1). With $\omega = kC$, the analysis falls back to the temporal instability and (5.1) becomes

$$\frac{\Phi_1^{(1)}}{\Phi_2^{(1)}} = -\frac{[(U_2+U_1)/2 - C_R + \beta/K^2]^2 - \frac{1}{4}(U_1-U_2)^2 + C_I^2 + iC_I(U_2-U_1)}{|(C-U_1+\beta/K^2)|^2} = Ae^{i\theta_p} \tag{5.2}$$

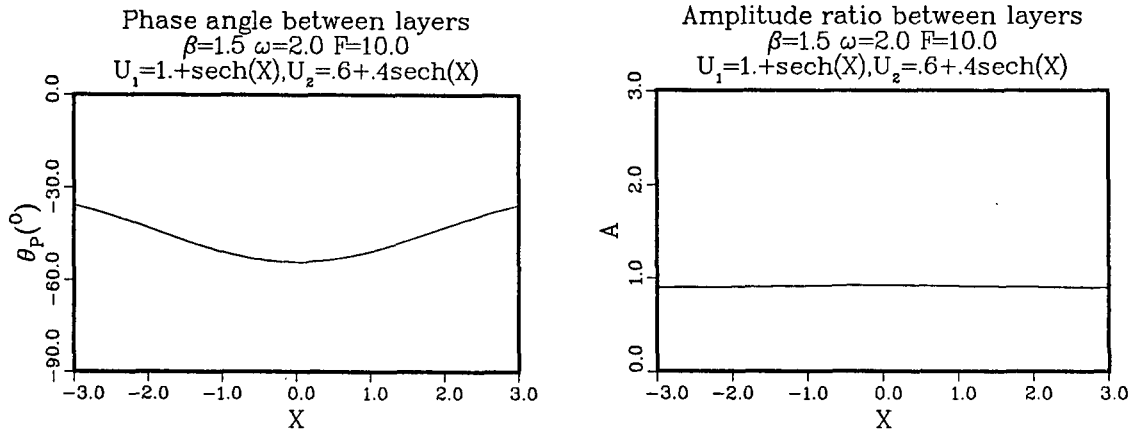

FIG. 11. (a) Phase angle; (b) amplitude ratio between the two layers for case 3 where the U_1 and U_2 profiles are in Fig. 9.

where C is the complex phase speed and $C = C_R + iC_I$. The phase angle θ_p in (5.2) is

$$\theta_p = \tan^{-1}\left[\frac{-C_I(U_1-U_2)}{-\frac{1}{4}(U_1-U_2)^2+[\frac{1}{2}(U_1+U_2)-C_R+\beta/K^2]^2+C_I^2}\right]. \tag{5.3}$$

and the amplitude A is

$$A = \frac{\{[(\frac{1}{2}(U_2+U_1)-C_R+\beta/K^2)^2-\frac{1}{4}(U_1-U_2)^2+C_I^2]^2+C_I^2(U_1-U_2)^2\}^2}{|C-U_1+\beta/K^2|^2}. \tag{5.4}$$

First, consider the situation when $\beta = 0$. From Eq. (7.11.9) in Pedlosky (1979),

$$C_R = \frac{1}{2}(U_1+U_2), \tag{5.5}$$

$$C_I = \pm\frac{1}{2}(U_1-U_2)\left[\frac{2F-K^2}{2F+K^2}\right]^{1/2}. \tag{5.6}$$

Introducing (5.5) and (5.6) into (5.3), the expression becomes

$$\theta_p = \tan^{-1}\left[\frac{2\cdot\left(\frac{2F-K^2}{2F+K^2}\right)^{1/2}}{\left[-1+\left(\frac{2F-K^2}{2F+K^2}\right)\right]}\right]. \tag{5.7}$$

Therefore, when $\beta = 0$, the phase difference does not depend explicitly on the shear, but only on the scale of the wave which is determined by k_0. With expression (3.16) evaluated for $m = 1$, we have

$$2F-K^2 = 2F-\pi^2-k_0^2,$$

$$2F+K^2 = 2F+\pi^2+k_0^2. \tag{5.8}$$

For very long wave, $k_0 \sim 1$, and $k_0^2 \sim O(1)$ which is an order smaller than $(2F - \pi^2)$ or $(2F + \pi^2)$. Thus, the variation of k_0 in the streamwise direction is even smaller and it can be neglected in (5.6). For example, when $k_0 = 1$

$$\theta_p \approx 55° \tag{5.9}$$

which is about the average phase angle in our results.

For higher frequency, the wavenumber increases and contribution from k in $2F - K^2$ is no longer small. If k is $\sim$3.5, then $2F - K^2 \sim 0$ and the phase angle between the layers approaches zero, which gives no instability. Since the wavenumber increases with the frequency, there is an upper bound of the frequency for spatial instability, as demonstrated by Merkine (1977) in his Fig. 4. The variation of θ_p will be larger for shorter waves with larger k_0.

As for the amplitude A, when $\beta = 0$ the expression (5.4) becomes identically equal to 1 when (5.5) and (5.6) are used. In other words, the amplitude A is totally independent of the shear and the scale of the waves when β equals zero.

When $\beta \neq 0$, Eq. (7.11.13) in Pedlosky (1979) gives

$$C_R = \frac{U_1+U_2}{2} - \frac{(K^2+F)}{K^2(K^2+2F)} \tag{5.10}$$

$$C_I = \pm\frac{1}{2K^2(K^2+2F)}\{4^2F^2-K^4U_s^2(4F^2-K^4)\}^{1/2} \tag{5.11}$$

$$\theta_p = \tan^{-1}\left[-\frac{C_I(U_1-U_2)}{\frac{1}{2}(U_1-U_2)^2+\left[\frac{F}{K^2(K^2+F)}\right]^2+C_I^2}\right] \tag{5.12}$$

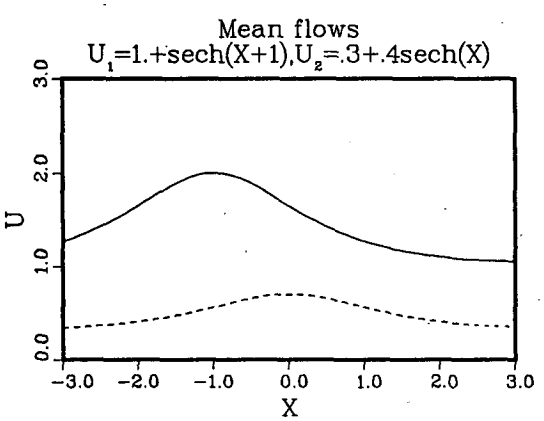

FIG. 12. U_1 and U_2 profiles for case 4.

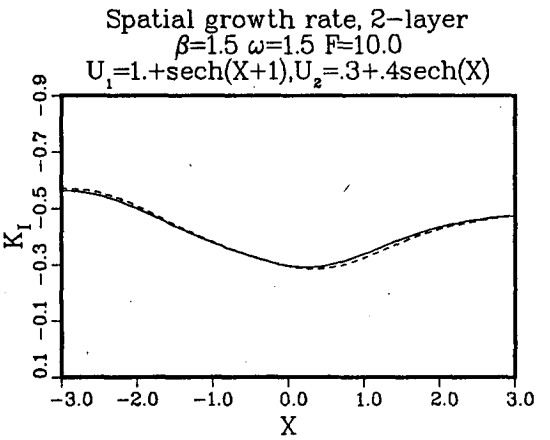

FIG. 13. Local (solid line) and streamwise (dashed line) spatial growth rate for case 4 as in Fig. 12.

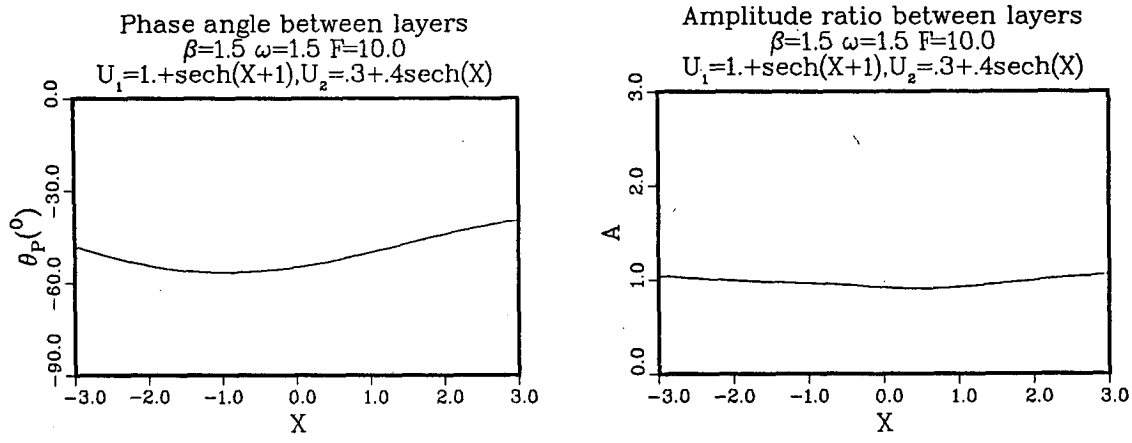

FIG. 14. (a) Phase angle; (b) amplitude ratio between the two layers for case 4 as in Fig. 12.

$$A=\frac{\left\{\left[\frac{\beta^2(2K^2+3F)^2}{K^4(K^2+2F)^2}-\frac{1}{4}(U_1-U_2)^2+C_I^2\right]^2+C_I^2(U_1-U_2)^2\right\}^{1/2}}{\left(\frac{\beta F}{K^2(K^2+2F)}-\frac{U_1-U_2}{2}\right)^2+C_I^2} \tag{5.13}$$

Now the variation of k_0 and the shear would have a larger effect on the variations of θ_p and A. When the shear is large, the β effect is comparatively small, and the variations of θ_p and A are small. If the shear is small, however, the β effect becomes important and variations of θ_p and A are large. For all the cases discussed in section 4, we have $\beta \neq 0$. In case 5, the minimum shear region is near $X = 0.5$, where both the phase angle and the amplitude variations are substantial and the streamwise effect is large in that region due to the lag effect. In case 2, the shear decreases toward the inflow and outflow regions, variations of the phase angle and the amplitude become large and the lag effect increases. For case 1, the streamwise variation of the shear is the same as in case 2, but the absolute shear value is much larger everywhere than in case 2. Therefore, the disturbance structure is more uniform and the lag effect is negligible. For the same reason, the minimum shear in case 4 ($X = 0.3$ in Fig. 12) is larger than the minimum shear in case 5 ($X = 0.5$ in Fig. 15). Consequently, the local vertical structure in case 4 does not show a large variation near the minimum shear region (compare Fig. 14 with Fig. 18).

To verify the above analysis, case 2 is recalculated with $\beta = 0$, keeping all other parameters unchanged. The variation in the vertical structure is greatly reduced, as can be seen by comparing Fig. 19 with Fig. 7. The reduced variation of the disturbance structure greatly reduces the lag effect as is evident in Fig. 20. The slight nonparallel effect in this case comes from the phase speed difference mechanism. As a further illustration, β is kept the same as in case 2, but the shear is increased

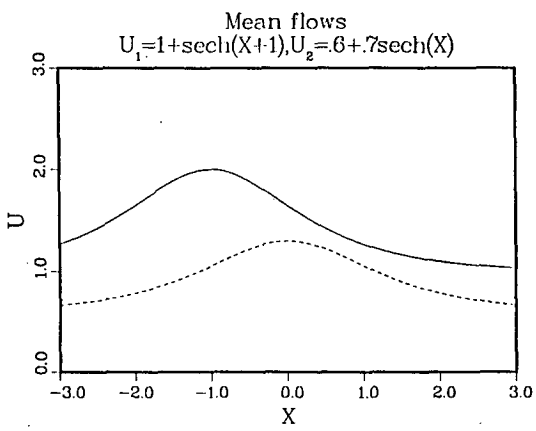

FIG. 15. U_1 and U_2 profiles for case 5.

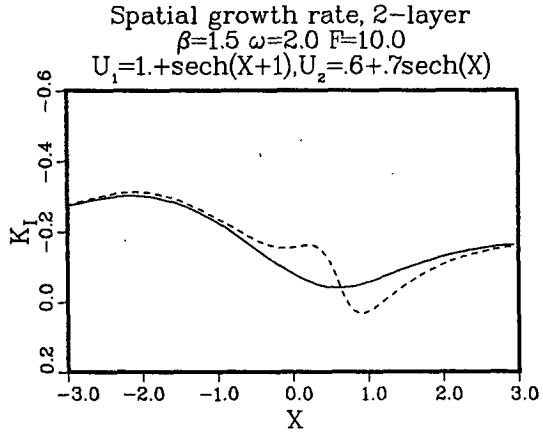

FIG. 16. Local (solid line) and streamwise (dashed line) spatial growth rate for case 5 as in Fig. 15.

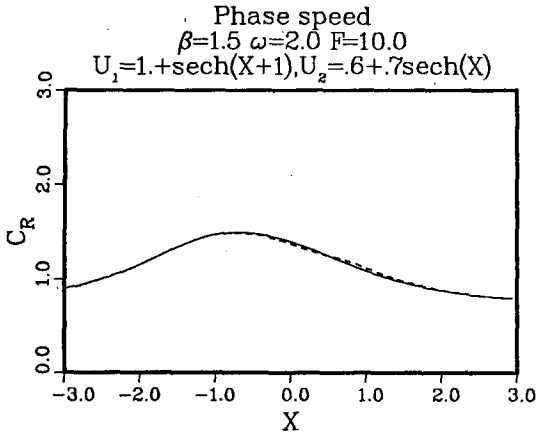

FIG. 17. Local (solid line) and streamwise (dashed line) phase speeds for case 5 as in Fig. 15.

by increasing the uniform part of the upper layer flow; i.e.,

$$U_1 = 1.5 + \mathrm{sech}(X),$$
$$U_2 = 0.9. \qquad (5.12)$$

As in Fig. 19, the variation of the local vertical structure (Fig. 21) is also greatly reduced as can be seen by comparison with Fig. 7, and the nonparallel effect in Fig. 22 is the same as in Fig. 20. Therefore, increasing the shear causes the same result as decreasing the β effect. Both of them will reduce the variation of the vertical structure with respect to the variation of the shear, rendering the lag effect less unimportant.

6. Discussion

In this paper, the two-scale technique is applied to study the nonparallel effects with basic flows which vary slowly in the streamwise direction in the two-layer baroclinic model. Different streamwise variations of the basic flows are analyzed, including vertical shifting of the maximum wind speed region in the two layers. The difference between the nonparallel flow solution and the parallel flow solution which is determined locally, is explained successfully with the mechanisms discussed previously by Peng and Williams (1986a) for the barotropic model. The nonparallel contribution is mainly dominated by the lag effect, which is determined by the streamwise variation of the vertical disturbance structure. This vertical structure is the ratio between the disturbance solutions for the upper and lower layers and is represented by its amplitude and the phase angle. The lag effect is significant when both the amplitude and the phase angle change substantially in the streamwise direction.

Variations of the vertical structure are analyzed by using the temporal instability, because $\omega = kC$ precisely links the temporal and spatial growth for the present model. When the β-effect is excluded, or the magnitude of the shear is large, the disturbance structure is almost uniform in the streamwise direction irrespective of a substantial variation of the shear. In this case, the lag effect is small, and the locally determined solution is very close to the total solution. The lag effect is important when the shear is small. Therefore, the nonparallel correction is more important during the summer than the winter for the atmospheric jets.

Grotjahn (1984b) used numerical integration of a high-resolution multilevel spectral model to study baroclinic instability in an environment with long waves. In his uniform basic state, the vertical shear had a nondimensional value of 1 corresponding to our scaling. In his experiment which corresponded most closely to ours, the vertical shear increased along the jet. For this experiment he found that the disturbance vertical structure did not change appreciably downstream (Fig. 5, Grotjahn, 1984b). Although he did not compare the local and streamwise varying solutions, his finding that the disturbance structure did not vary downstream agrees with our result for large vertical shear. The consistency between his results and ours may not be fortuitous and it may indicate that our analysis concerning the vertical structure variation can

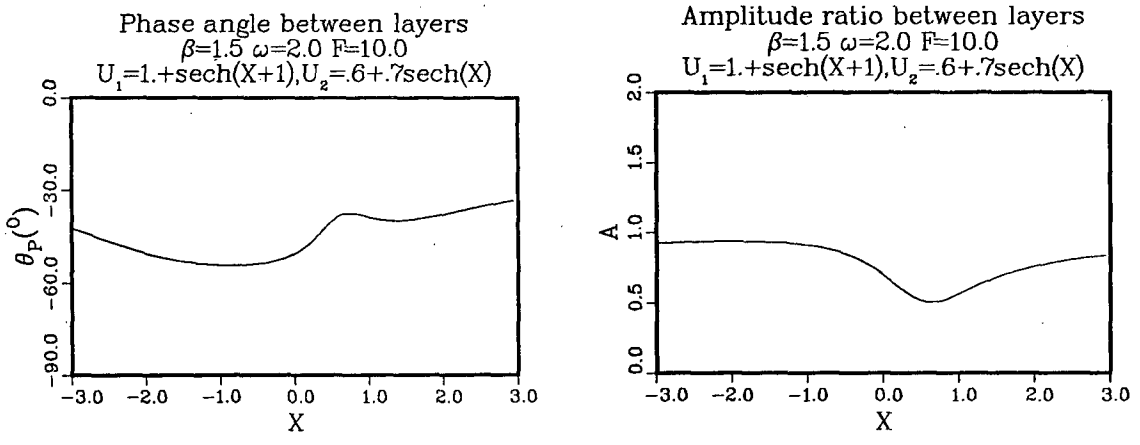

FIG. 18. (a) Phase angle; (b) amplitude ratio between the two layers for case 5 as in Fig. 15.

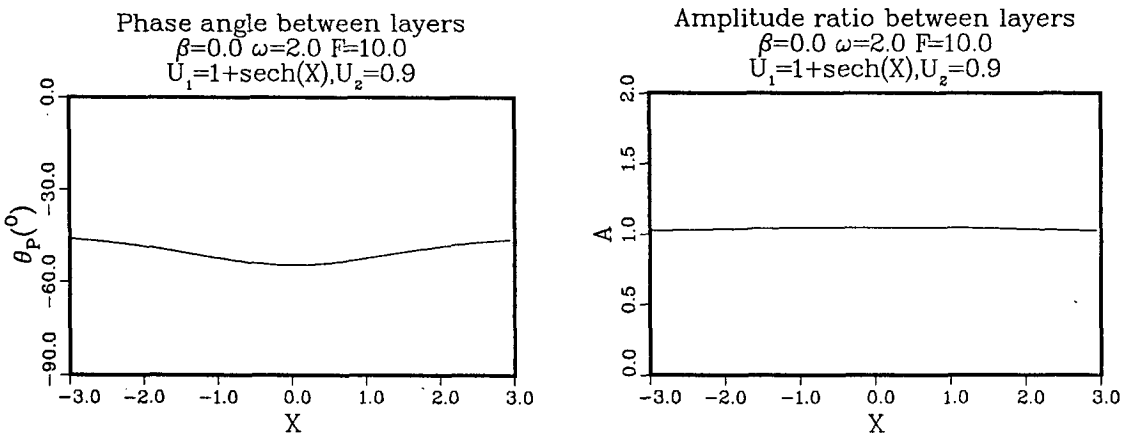

FIG. 19. (a) Phase angle; (b) amplitude ratio between the two layers with the mean flows U_1 and U_2 the same as in case 2 except $\beta = 0$.

be applied to the continuously stratified flows. More studies are needed to verify this.

As mentioned in the introduction, Pierrehumbert (1984) studied the time evolution of a baroclinic disturbance in the two-layer model in a basic flow with streamwise variation. The results from the numerical integration were compared with an analytical solution, which was obtained locally using parallel flow theory. No correction for the streamwise variation in the mean flow was included. However, the numerical results contain the streamwise effect, and the closeness of these solutions agrees with our results.

In an early study, Ling and Reynolds (1973) examined the nonparallel effect for several different types of shear flow with streamwise variation. The higher order correction was found to be important for some situations and not for others. No physical reason was given to explain their results.

From the climatological data analyzed by Blackman et al. (1978) and Lau (1979), the location of the maximum amplitude for the eddies is shifted downstream from the region of maximum shear. Frederiksen (1978, 1979, 1980) and Niehaus (1980, 1981) superimposed a long wave upon a zonally uniform flow. The temporal approach was used by them with cyclic boundary conditions. This procedure yields a single growth rate and an eigenfunction whose envelope varies in the streamwise direction. The exact reason for the downstream shifting of the envelope was not explained explicitly. Pierrehumbert (1984) elucidated this point. In his study, where the basic flow supported absolute instability in some region, the frequency obtained at the maximum absolute instability dominated the whole domain. The complex wavenumber obtained locally with that fixed frequency from the dispersion relation determined the spatial structure and spatial growth (or decay). The wave envelope had a maximum amplitude at the point where the spatial growth (the imaginary part of the wavenumber) vanished; i.e.,

$$\frac{1}{\psi}\frac{\partial \psi}{\partial x} = -k_I. \tag{6.1}$$

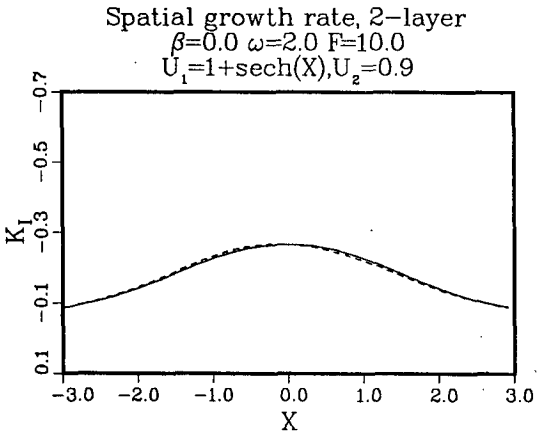

FIG. 20. Local (solid line) and streamwise (dashed line) spatial growth rate with the mean flow U_1 and U_2 the same as in case 2 except $\beta = 0$.

In barotropic studies with streamwise varying mean flows, Tupaz et al. (1978) and Williams et al. (1984) found spatially growing disturbances with a maximum amplitude downstream from regions of maximum temporal instability. Tupaz et al. integrated the equation numerically with periodic forcing on the upstream boundary. After an adjustment phase, the entire field began to oscillate with the forced frequency, since in this case there was no absolute instability. For a basic flow that does not support absolute instability, a train of waves can move into the region that is baroclinically unstable. The disturbances then grow spatially as they propagate downstream and the amplitude of the wave packet increases with distance. At the point where the spatial growth rate vanishes, the amplitude reaches a maximum. The frequency that will dominate is the one that has the largest overall spatial growth, while if there is absolute instability somewhere in the domain, the frequency would be the one excited by the maxi-

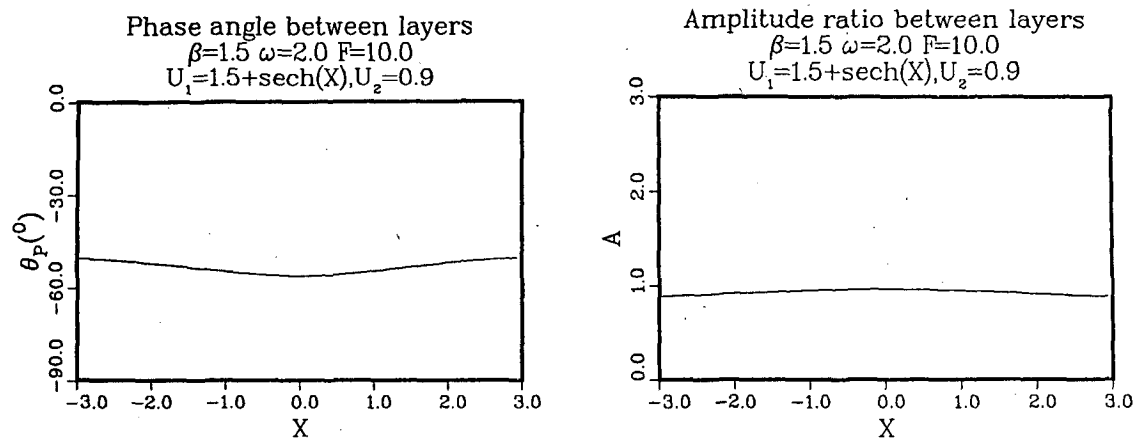

FIG. 21. (a) Phase angle; (b) amplitude ratio between the two layers for U_1 and U_2 profiles given in (5.12) and $\omega = 1.5$.

mum absolute instability as discussed in Pierrehumbert (1984). Nevertheless, with or without absolute instability, the downstream shifting of the maximum amplitude of the wave envelope is demonstrated clearly by the spatial growth. From the pure temporal instability approach, it is not clear how this can be demonstrated.

Pedlosky (1976) carried out a finite amplitude study with the two-layer quasi-geostrophic model of a flow with an abrupt change in the baroclinic stability properties. On the upwind side of the change there was a uniform weak instability and on the downwind side the flow was stable. He also considered the reversed situation. Our study differs in that we allow a smooth transition and a finite change in the stability parameter over a large distance. In his steady amplitude solutions he used the spatial growth approach. When his equations are linearized, the maximum amplitude occurs a short distance into the stable region. There is a lag effect which comes from the matching condition when the flow passes from the unstable region to the stable region, but he did not discuss it in the linear context.

In the present study the $O(\epsilon)$ correction to the local spatial growth rate from the streamwise variation in the mean flow is small. This suggests that under more general conditions the local spatial growth solution will give a good first estimate of the behavior as long as the streamwise scale is large compared with the disturbance scale. On the other hand, since the corrections are very small when the shear is not too small, the theory should be applicable to somewhat smaller scale streamwise variations, i.e., where ϵ is not small. Consider, for example, the cyclogenesis problem in the lee of a long mountain range like the Rocky Mountains. Suppose that the baroclinicity is enhanced near the mountains. Since the phase speed may also increase, the local spatial growth rate may not increase, as can be seen from (4.7). Even if the growth rate is increased, the effect on the disturbance amplitude will be small if the width of the more unstable area is small. If a more realistic model were used (mean flow with horizontal shear, more vertical layers, explicit topography, etc.), the lag effect is small, and the locally-determined solution is (1986) would be more important. This lag effect would then further reduce the enhanced instability near the topography, since the disturbance would not have enough time in the region which has a larger local growth rate to take advantage of the enhanced instability.

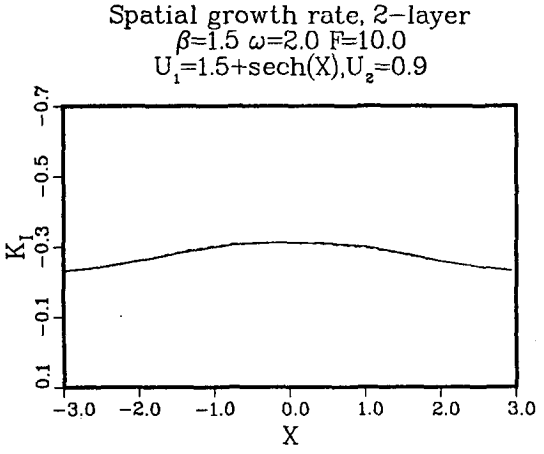

FIG. 22. Local (solid line) and streamwise (dashed line) spatial growth rate corresponding to Fig. 21.

Acknowledgments. The authors wish to thank Dr. William Blumen for reading the manuscript and for useful discussions on the research. The first author was supported during part of this research by a National Research Council Associateship. The NRC Associate Program is supported by the Naval Postgraduate School Foundation Research Program, which is funded by the Chief of Navy Material. This research was also supported by the Division of Atmospheric Sciences, National Science Foundation under Grants ATM 83-15175 and ATM 84-44699. The Manuscript was care-

fully typed by Miss K. Lee and the numerical computations were carried out at the W. R. Church Computer Center at the Naval Postgraduate School.

APPENDIX

Expression for H_1 and H_2 in Eq. (3.24) obtained from the solvability condition imposed on O(ϵ) problem.

$$H_1=\frac{1}{i(U_1k_0-\omega)F}\Bigg\{k_1[-2i\omega k_0\Phi_1+3ik_0{}^2\Phi_1$$
$$+iU_1m^2\pi^2\Phi_1-i\Phi_1\beta+iF(U_2\Phi_1-U_1\Phi_2)+2rk_0\Phi_1]$$
$$-(\omega+ir)\left(2k_0\frac{\partial\Phi_1}{\partial X}+\Phi_1\frac{\partial k_0}{\partial X}\right)+3k_0U_1\left(k_0\frac{\partial\Phi_1}{\partial X}+\Phi_1\frac{\partial k_0}{\partial X}\right)$$
$$+U_1m^2\pi^2\frac{\partial\Phi_1}{\partial X}-\beta\frac{\partial\Phi_1}{\partial X}+F\left(U_2\frac{\partial\Phi_1}{\partial X}-U_1\frac{\partial\Phi_2}{\partial X}\right)\Bigg\}$$

$$H_2=\frac{1}{i(U_2k_0-\omega)F}\Bigg\{k_1[-2i\omega k_0\Phi_2+3ik_0{}^2\Phi_2$$
$$+iU_2m^2\pi^2\Phi_2-i\Phi_2\beta+iF(U_1\Phi_2-U_2\Phi_1)+2rk_0\Phi_2]$$
$$-(\omega+ir)\left(2k_0\frac{\partial\Phi_2}{\partial X}+\Phi_2\frac{\partial k_0}{\partial X}\right)+3k_0U_2\left(k_0\frac{\partial\Phi_2}{\partial X}+\Phi_2\frac{\partial k_0}{\partial X}\right)$$
$$+U_2m^2\pi^2\frac{\partial\Phi_2}{\partial X}-\beta\frac{\partial\Phi_2}{\partial X}+F\left(U_1\frac{\partial\Phi_2}{\partial X}-U_2\frac{\partial\Phi_1}{\partial X}\right)\Bigg\}$$

Expression for S_1 and S_2 in (3.26) for the O(ϵ) wavenumber k.

$$S_1=-i\Bigg\{\frac{1}{(U_1k_0-\omega)}\left[-(\omega+ir)\frac{\partial k_0}{\partial X}+3k_0U_1\frac{\partial k_0}{\partial X}\right.$$
$$\left.-FU_1\frac{\partial R}{\partial X}\right]+\frac{1}{(U_2k_0-\omega)}\left[-(\omega+ir)\left(2k_0\frac{1}{R}\frac{\partial R}{\partial X}+\frac{\partial k_0}{\partial X}\right)\right.$$
$$+3k_0U_2\left(\frac{k_0}{R}\frac{\partial R}{\partial X}+\frac{\partial k_0}{\partial X}\right)+\frac{U_2m^2\pi^2}{R}\frac{\partial R}{\partial X}$$
$$\left.-\frac{\beta}{R}\frac{\partial R}{\partial X}+\frac{FU_1}{R}\frac{\partial R}{\partial X}\right]\Bigg\}$$

$$S_2=\Bigg\{(2\omega k_0-3k_0{}^2-U_1m^2\pi^2+\beta+2irk_0)\left(\frac{1}{(U_1k_0-\omega)}\right.$$
$$\left.-\frac{1}{(U_2k_0-\omega)}\right)-\frac{F(U_2-U_1R)}{(U_1k_0-\omega)}-\frac{F(U_1-U_2/R)}{(U_2k_0-\omega)}\Bigg\}.$$

REFERENCES

Blackman, M. L., J. M. Wallace, N. Lau and S. L. Mullen, 1977: An observational study of the Northern Hemisphere wintertime circulation. *J. Atmos. Sci.*, **34**, 1040–1053.

Benney, D. J., and S. Rosenblat, 1964: Stability of spatially varying and time-dependent flows. *Phys. Fluids*, **7**, 1385–1386.

Briggs, R. J., 1964: *Electron-Stream Interaction with Plasma.* Chapter 2, the MIT Press.

Charney, J. G., 1947: The dynamics of long waves in a baroclinic westerly current. *J. Meteor.*, **4**, 135–163.

Drazin, P. G., 1974: On a model of instability of a slowly varying flow. *Quart. J. Mech. Appl. Math.*, **27**, 69–83.

Eady, E. T., 1949: Long waves and cyclone waves. *Tellus*, **1**, 33–52.

Frederiksen, J. S., 1978: Instability of planetary waves and zonal flows in two-layer models on a sphere. *Quart. J. Roy. Meteor. Soc.*, **104**, 841–872.

——, 1979: The effect of long planetary waves on the regions of cyclogenesis. *J. Atmos. Sci.*, **36**, 195–204.

——, 1980: Zonal and meridional variations of eddy fluxes induced by long planetary waves. *Quart. J. Meteor. Soc.*, **106**, 63–84.

Grotjahn, R., 1984a: Baroclinic instability in a long-wave environment. Part I: review. *Quart. J. Meteor. Soc.*, **110**, 663–668.

——, 1984b: Baroclinic instability in a long-wave environment. Part II: Ageostrophic energy conversions. *Quart. J. Meteor. Soc.*, **110**, 669–693.

Lau, N., 1979: The structure and energetics of transient disturbances in the Northern Hemisphere wintertime circulation. *J. Atmos. Sci.*, **36**, 982–995.

Ling, C.-H., and W. C. Reynolds, 1973: Nonparallel flow corrections for the stability of shear flows. *J. Fluid Mech.*, **59**, 571–591.

Merkine, L., 1977: Convective and absolute instability of baroclinic eddies. *Geophys. Astrophys. Fluid Dyn.*, **9**, 129–157.

——, and M. Shafranek, 1980: The spatial and temporal evolution of localized unstable baroclinic disturbances. *Geophys. Astrophys. Fluid Dyn.*, **16**, 174–206.

——, and R. Balgovind, 1983: Barotropic instability of weakly nonparallel zonal flows. *Geophys. Astrophys. Fluid Dyn.*, **25**, 157–190.

Nayfeh, A. H., 1979: *Introduction to Perturbation Techniques.* Wiley & Sons, 519 pp.

——, W. S. Saric and D. T. Mook, 1974: Stability of nonparallel flows. *Arch. Mech.* **26**, 401–406.

Niehaus, M. C. W., 1980: Instability of nonzonal baroclinic flows. *J. Atmos. Sci.*, **37**, 1447–1463.

——, 1981: Instability of nonzonal baroclinic flows: Multiple-scale analysis. *J. Atmos. Sci.*, **38**, 974–987.

Oort, A. H., 1983: Global atmospheric circulation statistics, 1958–1973. NOAA *Prof.* Paper 14. 180 pp.

Pedlosky, J., 1976: Finite-amplitude baroclinic disturbances in downstream varying currents. *J. Phys. Oceanogr.*, **6**, 335–344.

——, 1979: *Geophysical Fluid Dynamics.* Springer-Verlag, 624 pp.

Peng, M. S., and R. T. Williams, 1986: Spatial instability of the barotropic jet with slow streamwise variation. *J. Atmos. Sci.*, **43**, 2430–2442.

——, and ——, 1987: On the transformations between the temporal and spatial growth rate. Submitted to *J. Atmos. Sci.*

Phillips, N. A., 1951: A simple three-dimensional model for the study of large-scale extratropical flow patterns. *J. Meteor.*, **8**, 381–394.

Pierrehumbert, R. T., 1984: Local and global baroclinic instability of zonally varying flow. *J. Atmos. Sci.*, **41**, 2141–2162.

Thacker, W. C., 1976: Spatial growth of gulf stream meanders. *Geophys. Fluid Dyn.*, **7**, 271–295.

Tupaz, J. B., R. T. Williams and C.-P. Chang, 1978: A numerical study of barotropic instability in a zonally varying easterly jet. *J. Atmos. Sci.*, **35**, 1265–1280.